Polymer 205 (2020) 122868

Contents lists available at ScienceDirect

Polymer

journal homepage: http://www.elsevier.com/locate/polymer

Kinetic study of alkyl methacrylate polymerization in nanoporous confinement over a broad temperature range

Qian Tian, Haoyu Zhao, Sindee L. Simon *

Department of Chemical Engineering Texas Tech University, Lubbock, USA

ARTICLE INFO

Keywords:
Nanoconfinement
Free radical polymerization
Reaction kinetics

ABSTRACT

The effect of nanoconfinement on the free radical polymerization of ethyl methacrylate (EMA) and n-butyl-methacrylate (BMA) with di-*tert*-butyl peroxide (DtBP) initiator is investigated over a wide temperature range from 80 to 190 °C using differential scanning calorimetry. The effective rates are similar for the two bulk monomers although the BMA reacts approximately 11% faster at 95 °C. For nanoconfined cases, the initial reaction rate for monomer confined in the pores of controlled pore glass is enhanced, with larger effects observed in native pores compared to pores in which the native silanol was converted to trimethyl silyl. The onset of autoacceleration also occurs earlier under nanoconfinement, with decreases in both the conversion and the time required to reach autoacceleration, x_{gel} and t_{gel}, respectively, and larger changes for the native pores. The induction time follows Arrhenius behavior and increases under nanoconfinement. At polymerization temperatures above 160 °C, depropagation becomes important as the ceiling temperature is approached and seems to be more pronounced under nanoconfinement than in the bulk.

1. Introduction

Nanoconfinement is known to affect the physical properties of polymers, including the glass transition temperature [1–3], the molecular weight and the polydispersity of polymers synthesized under nanoconfinement [4–8], and polymerization reaction kinetics [9–20]. In the case of nanopore-confined step growth reactions, including phenolic resins [9], cyanate esters [10–12], isocyanates [13], and epoxies [14], polymerization kinetics are generally accelerated, except in the case of solid state reactions [15], with the acceleration attributed either to catalysis by functional groups on the pore surface or due to monomer layering at the pore surface in the absence of catalytic effects. On the other hand, for the nanoconfined free radical polymerization of methyl methacrylate (MMA) in controlled pore glasses (CPG) recently studied in our laboratory by differential scanning calorimetry (DSC) [8,16], the kinetics were found to be accelerated due to two effects: i) an earlier onset of autoacceleration presumed to arise from decreased chain diffusivity leading to a decreased rate of termination and ii) an increased rate of propagation in native pores presumed to result from specific interactions between the monomer and the silanol groups on the pore surface. The specific interactions also seem to orient the growing chain end leading to a significant increase in isotacticity [8]. In addition, the enhanced autoacceleration was found to result in an increase in the number-average and weight-average molecular weight and a decrease in the polydispersity index (PDI) relative to bulk values [8], consistent with earlier and more recent work from other groups [4–6,17,18,21]. Mijangos and coworkers [19] also found that MMA polymerization in anodic aluminum oxide (AAO) templates is accelerated, but in their case, the acceleration was accompanied by a reduction in molecular weight compared to bulk conditions. Hence, they attributed their results to a higher initiator decomposition rate in the early stages of polymerization and increased termination in the latter stages of the reaction; a similar increase in the rate of termination was invoked to explain a reduction in polymerization rate by others in a nanoconfined liquid crystal structure [20]. Notwithstanding these two cases, the expected decrease in chain diffusivity under nanoconfinement [22] seems to generally dominate, leading to a decrease in termination rate and enhanced autoacceleration [16,23], as well as decreases in the rate of degradation in nanoconfined polystyrene and in poly(methyl methacrylate) [21,24].

For free radical polymerization in bulk conditions, depropagation becomes more important with increasing reaction temperature and decreasing monomer concentration as the ceiling temperature is approached [25–27]. With a pulsed-laser technique, Hutchinson and

* Corresponding author.
E-mail address: Sindee.Simon@ttu.edu (S.L. Simon).

https://doi.org/10.1016/j.polymer.2020.122868
Received 20 April 2020; Received in revised form 9 July 2020; Accepted 27 July 2020
Available online 28 July 2020

coworkers [26] were able to quantify the temperature dependences of the propagation and depropagation rate constants for several methacrylates, including n-butyl-, cyclohexyl-, isobornyl- and 2-hydroxypropyl-, n-dodecyl-methacrylate, in both bulk and solution. The equilibrium conversion of MMA was also observed to decrease with increasing temperature in our own work, and this effect was found to be more pronounced under nanoconfinement [28].

The objective of this work is to study the nanoconfined polymerization of two alkyl methacrylates in controlled pore glasses over a broad temperature range by DSC in order to understand how nanoconfinement affects the initial rate of polymerization, autoacceleration, and depropagation. In this work, we choose to study ethyl- and n-butyl-methacrylate (EMA and BMA) rather than the methyl methacrylate (MMA) used in our previous works [8,16,28] because of their higher boiling points, lower volatility, and lower glass transition temperatures. In addition, a different initiator, di-*tert*-butyl peroxide (DtBP), which initiates the reaction more slowly than the 2,2′-azobis(2-methylpropionitrile) (AIBN), is used in order to facilitate the measurements at high temperatures.

2. Experimental methodology

2.1. Materials

Ethyl- and n-butyl-methacrylate monomers (Sigma Aldrich, 99%, containing 10 ppm monomethyl ether hydroquinone as inhibitor) were purified with a prepacked column (Sigma Aldrich, No. 306312) to remove the inhibitor, and then the monomers were mixed with 0.5 wt % di-*tert*-butyl peroxide (Sigma Aldrich, 98%) initiator at room temperature to form a homogeneous solution. Solutions were stored in a freezer at −20 °C with desiccant prior to use. Less than 1% conversion accumulated during mixing and after two months of storage according to a calculation based on the reaction model.

The media used for nanoconfinement is controlled pore glass (CPG, Millipore) with two pore diameters of 8.1 ± 0.7 nm and 50 ± 1.9 nm. The specifications of CPG are listed in Table 1. Two different pore surface chemistries were also used, following the procedures from Jackson and McKenna [29]. The so-called "native" pores are cleaned with nitric acid (Mallinckrodt Chemicals, 68–70%) at 110 °C, rinsed with nanowater (Barnstead Nanopure Infinity System, by Thermo Scientific) until neutral, and then dried under vacuum (737 mm Hg) at 285 °C for 24 h. The "silanized" pores were obtained by immersing the cleaned CPG in hexamethydisilazane (Sigma Aldrich, 99.9%) at 55 °C for 20 h, rinsing well with chloroform, and then drying at 120 °C under vacuum (737 mm Hg) for 24 h. The silanization does not significantly change the pore size or pore size distribution of CPG [30]. After the treatment, the native pores have -SiOH groups on the surface; whereas the silanized pores are functionalized by trimethylsilyl groups, -Si(CH_3)$_3$. The native and silanized CPGs were stored under desiccant prior to use.

2.2. DSC measurements

A Mettler-Toledo DSC 1 with an ethylene glycol cooling system and nitrogen purge gas was used to study the reaction kinetics of ethyl- and butyl-methacrylate free radical polymerizations. Samples were prepared in 20 μL hermetic pans (PerkinElmer) under a nitrogen blanket. Similar to previous work [16], pore fullness ranged from 70% to 95% based on the specific volume of the CPG. The DSC temperature was calibrated with indium and liquid crystal (+)-4-*n*-hexylophenyl-40-(20-methylbutyl)-biphenyl-4-carboxylate (CE-3) at 10 K/min, and the enthalpy was calibrated with indium only. An isothermal calibration was performed with indium at 0.1 K/min [31]. To minimize systematic errors, an indium check was performed on a daily basis.

Table 1
Specifications of CPGs, as provided by the manufacturer.

Product name	Mean pore diameter (nm)	Pore diameter distribution (%)	Specific pore volume (cm^3/g)	Specific surface area (m^2/g)
CPG75C	8.1	9.0	0.49	197
CPG00500B	50.0	3.7	1.10	51

Polymerizations were carried out isothermally for temperatures ranging from 80 to 190 °C for EMA and from 90 to 190 °C for BMA. Reproducibility was examined up to five times for certain reaction temperatures. After the isothermal run, the sample was cooled to room temperature at 10 K/min, and then a dynamic heating scan to 180 °C at 10 K/min was performed on selected samples to check for residual heat. No residual heat was observed for any sample. In our previous work on equilibrium free radical MMA polymerization, a two-step temperature history had to be performed in order to avoid high reaction rates that can potentially cause leakage of the DSC pans [28]. In the current system, less than 1% weight loss was observed during polymerization, even with a one-step temperature history, based on measurements of the sample mass before and after runs. Thus, the lower volatility monomers coupled with a slower initiator prevented the high reaction rates that may lead to leakage of sample pans.

From the isothermal heat flow $\dot{Q}$, the time-dependent conversion x can be obtained:

$$x = \frac{1}{\Delta H_T}\int_0^t \dot{Q}dt \tag{1}$$

where the total heat of the polymerization ΔH_T for EMA is 505 ± 10 J/g based on six samples reacted at 80 and 95 °C, consistent with literature values of 506 ± 7 J/g and 528 ± 22 J/g [32,33]; the total heat of the polymerization for BMA is 419 ± 18 J/g based on seven samples reacted from 90 to 100 °C, also in good agreement with values of 397 ± 6 J/g, 408 ± 3 J/g, and 421 ± 9 J/g reported in the literature [33–35].

3. Results

Heat flow during isothermal polymerization at three reaction temperatures is plotted in Fig. 1 for representative EMA and BMA samples as a function of time after subtracting the induction time (t_{ind}), which depends on temperature and confinement, as will be discussed later. For both EMA and BMA, the initial reaction rate decreases with decreasing polymerization temperature as indicated by a smaller initial heat flow. Autoacceleration is observed as the long-time exothermic peak, for example, at approximately 400 and 1750s for bulk EMA polymerization at 150 and 120 °C, respectively. Autoacceleration, also known as the Tromsdorff effect, is due to the increase in viscosity as conversion increases, resulting in a decrease in chain diffusivity and an increase in the relative rate of propagation over termination. Since the viscosity increases as temperature decreases the exothermic peak associated with autoacceleration, which is imperceptible at 180 °C, becomes more and more significant at lower temperatures. For the samples confined in 8 nm CPG pores, the times required to reach autoacceleration and to complete the reaction decrease compared to the bulk at temperatures of 120 and 150 °C, as shown in Fig. 1, consistent with our previous results for MMA [16]. For the same reaction environment, the EMA polymerization takes less time compared with the BMA polymerization due to a more pronounced autoacceleration effect.

The effective rate constant can be obtained from the data in Fig. 1 after transposing to conversion x versus time and applying a first-order reaction model [36]:

$$R_{overall} = -\frac{d[M]}{dt} = k_{eff}[M] \tag{2}$$

$$-\ln(1-x) = k_{eff}t \tag{3}$$

where $R_{overall}$ is the overall reaction rate, [M] is the monomer concen-

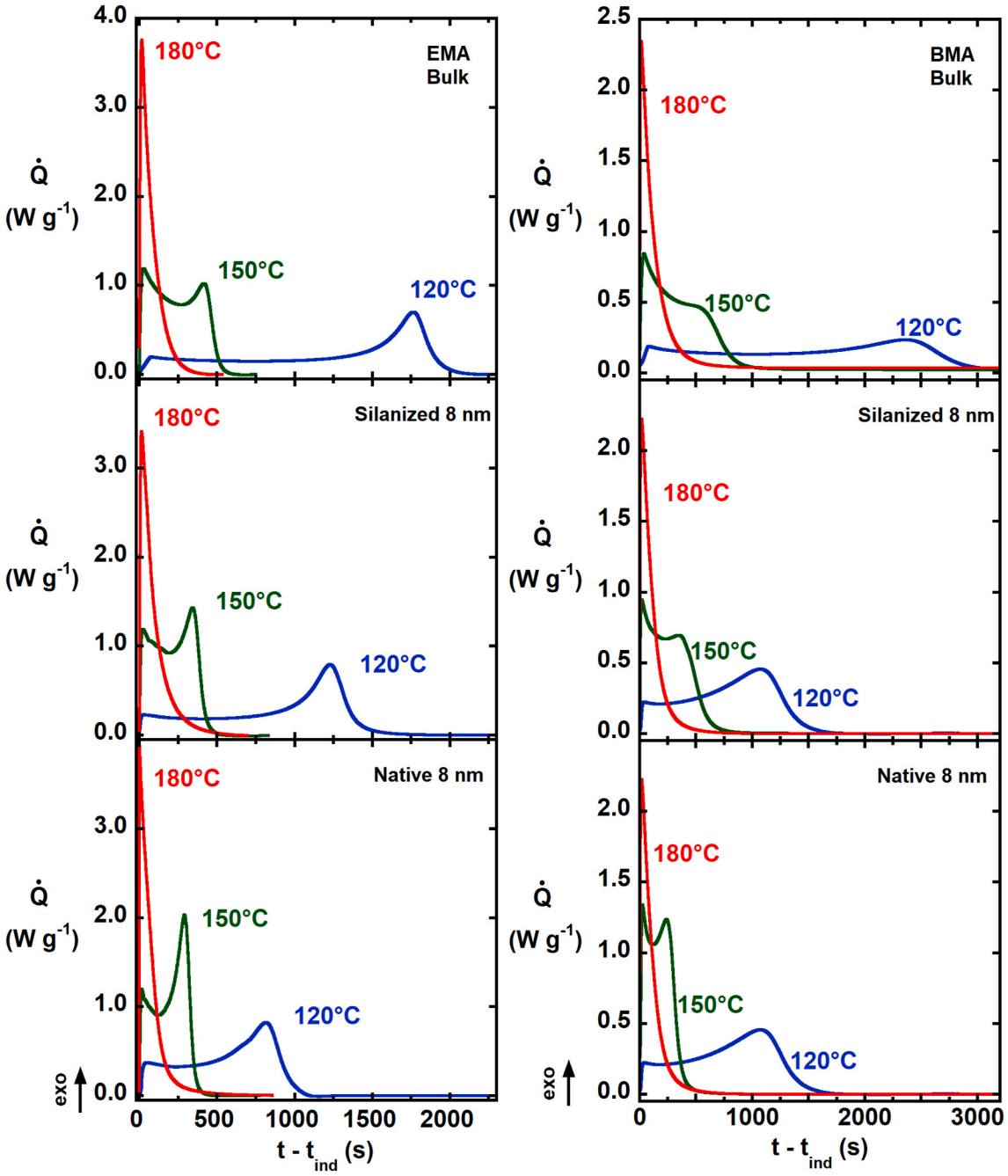

Fig. 1. Heat flow versus time for isothermal polymerization at three reaction temperatures for representative samples in bulk and in silanized and native 8-nm diameter CPG pores. The time scales for the two materials differ with the time range being 2600 s for EMA and 3250 s for BMA; the y-axis scales also differ.

tration, k_{eff} is the effective rate constant, which is related to the concentration of free radicals, as well as the specific reaction rate constants for propagation (k_p), initiator dissociation (k_d), and termination (k_t). When the depropagation rate constant (k_{dp}) becomes important at high reaction temperatures, k_{eff} will also depend on k_{dp}. In this case, the reaction can be written as an equilibrium reaction:

$$\sim M_{n\cdot} + M \underset{k_{dp}}{\overset{k_p}{\rightleftharpoons}} \sim M_{n\cdot+1} \tag{4}$$

where $M_{n\cdot}$ and $M_{n\cdot+1}$ are the growing radical chain of length n and $n+1$ and M is the monomer. The depropagation effect can be accounted for by revising equation (3) noting that at equilibrium, the forward and back reaction rates are equal such that,

$$-\ln(x_\infty - x) = k_{eff} t \tag{5}$$

where x_∞ is the conversion at equilibrium. For all temperatures studied, the first-order model fits the data well at low conversions, from 2 to 20%, where the reaction is kinetically controlled and the steady state approximation holds. This approach has been validated in two ways. First, the analysis was also performed over a narrower conversion range, from 2 to 10%, and the rate constant was found to be the same, with an average difference of 3.6% and a maximum difference of 13% for one point at the highest reaction temperature. Given that the rate constant varies by over two orders of magnitude, these differences are inconsequential. In addition, the rate of free radical generation was calculated and found to decrease by less than 3% relative to the initial rate at 20% conversion for reaction at 150 °C and to decrease less than 16% at

180 °C, thus indicating sufficient initiator to maintain steady state over the conversion range in which we perform the analysis.

The resulting effective rate constants for bulk EMA and BMA are plotted versus reciprocal temperature in Fig. 2 (a) with results using Equation (3) ignoring the back reaction shown as filled symbols and those using Equation (5) considering the back reaction shown as open symbols. Below 160 °C, the effective rate is essentially the same for these two methods, but at higher temperatures, the effective rate constant is higher when the back reaction is taken into consideration. In addition, the effective rates are similar for the two monomers but the BMA reaction is approximately 11% faster at 95 °C. This result is consistent with the data in the literature which show that the apparent rate constant increases as the alkyl group length increases for n-alkyl methacrylates due to a decrease in the rate constant for termination with no change in the propagation rate [37–39]. The effect is stronger at lower temperatures [37–39], consistent with the small difference in the apparent activation energies which can be obtained from the Arrhenius plot:

$$k_{eff} = Ae^{\frac{-E_{app}}{RT}} \tag{6}$$

where A is the preexponential factor and E_{app} is the Arrhenius activation energy which, in the absence of the reverse reaction, is related to the activation energies for propagation (E_p), thermal decomposition (E_d) and termination (E_t) (i.e., $E_{app} = E_p + \frac{E_d}{2} - \frac{E_t}{2}$) [36]. From the slope of Fig. 2 (a), E_{app} of EMA and BMA are found to be 84 ± 1 kJ/mol and 81 ± 1 kJ/mol for bulk samples reacted up to 150 °C, consistent with the literature values ranging from 79 to 102 kJ/mol [36,40–43]; the reported error in E_{app} is the standard error of the fitted parameter.

In addition to the bulk reaction rates and activation energies, the conversion and time at the onset of autoacceleration for bulk EMA and BMA as a function of polymerization temperature are plotted in Fig. 2 (b) and (c), respectively. The conversion (x_{gel}) and time (t_{gel}) required to reach autoacceleration are defined as the point where the slope of conversion versus time abruptly increases. For both EMA and BMA, the time at the onset of autoacceleration decreases with increasing temperature as the reaction rate increases. On the other hand, the conversion at the onset of autoacceleration increases with increasing temperature presumably because the viscosity decreases with increasing temperatures due to both the intrinsic temperature effect and the fact that the polymer molecular weight decreases as temperature increases; the result is that a higher conversion is needed to impact the termination rate and cause autoaccleration as temperature increases. Comparing EMA to BMA, x_{gel} and t_{gel} are approximately the same, indicating that the length of the alkyl substituent does not significantly affect the relative onset of autoacceleration, although as mentioned previously and shown in Fig. 1, the increase in the reaction rate at autoacceleration is more pronounced for EMA. The similar values of x_{gel} and t_{gel} for the two systems is attributed to two issues: first, the T_gs of the two reaction mixtures at the onset of autoacceleration do not differ significantly, and second, the reaction temperature is far above T_g at the onset of autoacceleration. The Fox equation can be used to estimate the T_g of the systems at the onset of acceleration:

$$\frac{1}{T_{g,mix}} = \frac{1 - x_{gel}}{T_{g,monomer}} + \frac{x_{gel}}{T_{g,polymer}} \tag{7}$$

where $T_{g,mix}$, $T_{g,monomer}$ and $T_{g,polymer}$ are the glass transition temperature of the mixture, monomer and polymer, respectively. The T_gs of the monomers are assumed to be −141 and −142 °C for EMA and BMA, respectively, based on the empirical rule that $T_g/T_m = 2/3$ with melting temperatures of −75 and −76 °C for EMA [44] and BMA [45], whereas T_gs of PEMA and PBMA are taken to be 65 and 20 °C [46], respectively. The conversion to reach autoacccleration, x_{gel}, ranges from approximately 0.4 to 0.6. Accordingly, the glass transition temperature T_g at the lowest x_{gel} is approximately – 100 °C, whereas at the highest x_{gel}, it is −65 and −77 °C for the EMA and BMA mixtures, respectively. Thus, at

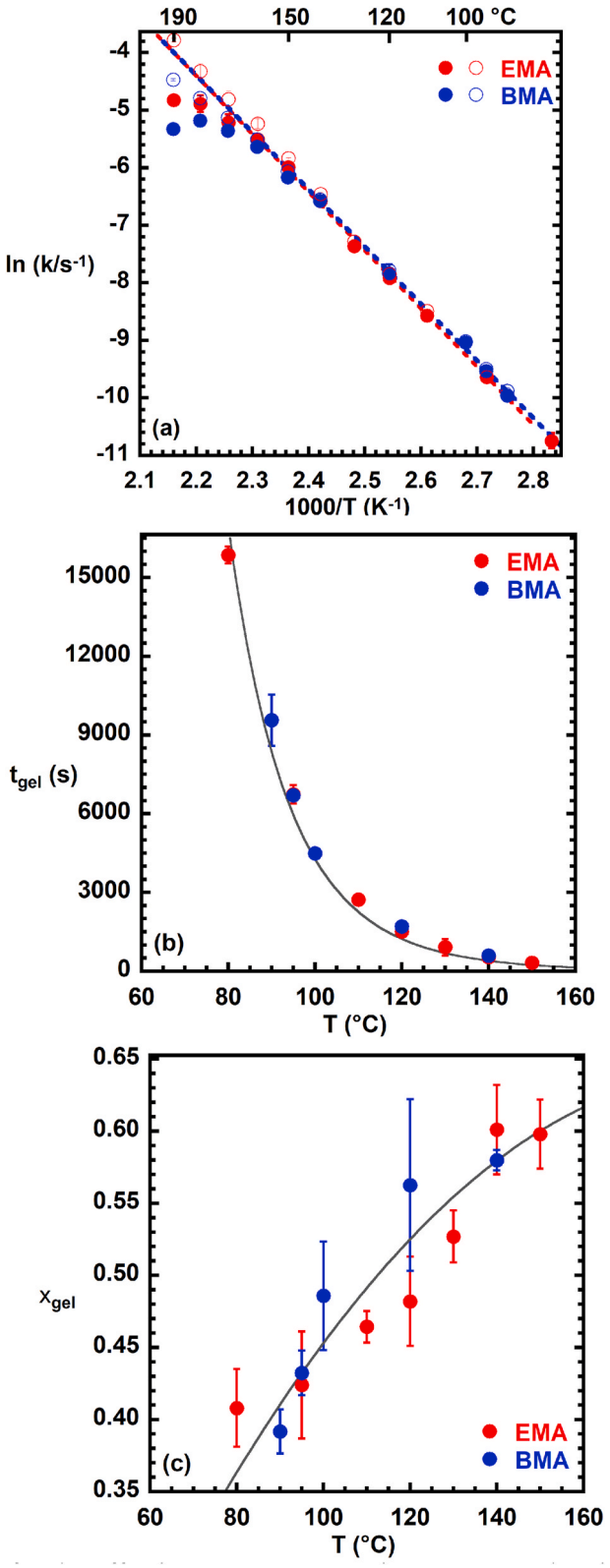

Fig. 2. (a) Arrhenius plot for the effective rate constant prior to autoacceleration for bulk EMA and BMA. Filled symbols represent data from Equation (3) ignoring the back reaction and open symbols represent data from Equation (5) considering the back reaction. (b) The time at the onset of autoacceleration and (c) the conversion at the onset of autoacceleration for bulk EMA and BMA samples as a function of polymerization temperature. The lines are only guides to the eye.

the onset of autoacceleration, the reaction temperature is over 150 °C above T_g. In this temperature regime, far above T_g, small differences in T-T_g do not have a large impact on mobility, and thus, the conversion at the onset of autoacceleration at a given temperature is not significantly different for EMA and BMA.

The influence of nanoconfinement on the reaction rate is compared with the bulk in Arrhenius plots versus reciprocal absolute temperature in Fig. 3 for EMA on the left and BMA on the right. The effective rate constants from Equation (3) (ignoring the back reaction) are shown as filled symbols and those from Equation (5) (considering for the back reaction) are shown as open symbols. As was the case for the bulk reactions, at temperatures below 160 °C, the two methods give essentially the same results. Also at temperatures below 160 °C, the effective rates are highest in the 8 nm-diameter native pores and lowest in bulk conditions for both EMA and BMA, with the rates for the reactions in silanized pores lying in between. The effective reaction rate shows an Arrhenius temperature dependence with the reaction rate increasing with increasing temperature. When the depropagation effect becomes significant at the highest temperatures, the k_{eff} values from Equation (3) are considerably lower than the Arrhenius fitting line, whereas the values from Equation (5) deviate considerably less. Also at the highest temperatures, k_{eff} from Equation (3) is slightly higher in bulk compared to nanopores, suggesting that the rate of depropagation accelerates more than that of propagation under nanoconfinement.

The apparent activation energies of EMA samples in silanized and native pores are 82 ± 2 kJ/mol and 81 ± 2 kJ/mol, respectively, indicating no change within the error of the measurements from the bulk, whereas the apparent activation energies of BMA samples in silanized and native pores are 70 ± 2 kJ/mol and 68 ± 2 kJ/mol, a reduction of approximately 15% from the bulk value. The changes in the apparent activation energy under nanoconfinement for EMA and BMA differ from that previously found for MMA polymerization in 13 nm CPG pores, where the material confined in silanized pores showed the same activation energy as the bulk and material confined in native pores showed a decrease in activation energy [16]. The differences are presumably related to the wider temperature range, different initiator and monomers, and/or smaller pore sizes used in the current work, as discussed in more detail in the discussion.

For both bulk and nanoconfined samples reacted above 160 °C, the reaction rate is lower than expected based on the Arrhenius temperature dependence at lower temperatures due to the increasing importance of depropagation effects at the highest temperatures, as shown by the increasing differences in the k_{eff} values calculated from Equations (3) and (5) with increasing temperature. Our finding is similar to that of Hutchinson and coworkers [26] for butyl methacrylate polymerizations, who found that depropagation became significant at 130 °C. Our higher temperature at which depropagation becomes important is attributed to the range of temperatures fitted for the Arrhenius parameters: in the current study, the Arrhenius plot is fitted in the temperature range of 80–150 °C, whereas in Hutchinson and coworkers' study, the Arrhenius plot was fitted for data from 10 to 90 °C. Hutchinson and coworkers were able to study such low temperatures because they used benzoin photoinitiator, whereas we used the thermal initiator DtBP, which is usually used at temperatures above 100 °C [36].

The ratio of the effective rate constants of the nanoconfined and bulk samples (k_{nano}/k_{bulk}) is plotted versus temperature in Fig. 4, where data for the silanized pores are shown on the left and for the native pores are on the right. Calculations based on Equation (3) are shown as filled symbols and those from Equation (5) are shown as open symbols. As temperature increases, the ratio k_{nano}/k_{bulk} decreases for both silanized and native cases, as was the case for our previous nanoconfined MMA polymerizations [16]. In the lower temperature range, the ratio of the effective rate constants k_{nano}/k_{bulk} is higher in native pores than in silanized pores presumably due to specific interactions between the monomer and the native silanol groups on the pore surface. The ratio is also larger in 8 nm pores compared to in 50 nm pores. In fact, for the silanized pores, the ratio of the effective rate constants k_{nano}/k_{bulk} of BMA reacted in 50 nm pores is the same as in bulk conditions, independent of reaction temperature. When comparing EMA with BMA, the degree of acceleration (k_{nano}/k_{bulk}) is larger for BMA than for EMA at a given temperature, indicating that the nanoconfinement effect is stronger in BMA since the bulk reactions have nearly similar rates as discussed earlier. Above 170 °C, the ratio k_{nano}/k_{bulk} becomes smaller than one, which indicates that nanoconfinement also accelerates depropagation, consistent with Fig. 3.

Changes to autoacceleration upon nanoconfinement can also be quantified by the conversion and time required to reach autoacceleration as a function of polymerization temperature, as shown in Fig. 5. The conversion at the onset of autoacceleration, x_{gel}, increases with increasing temperature for all temperatures in the bulk case, whereas under nanoconfinement, x_{gel} first increases with increasing temperature and then appears to either level off or decrease. The conversion at the onset of autoacceleration, x_{gel} is smaller under nanoconfinement than in bulk, and even smaller for samples in native pores compared to samples in silanized pores; this effect may be attributable to a higher effective viscosity in the silanized pores than in bulk and an even higher effective viscosity in the native pores. Such increases in effective viscosity have been observed for nanoconfined systems, both experimentally and by

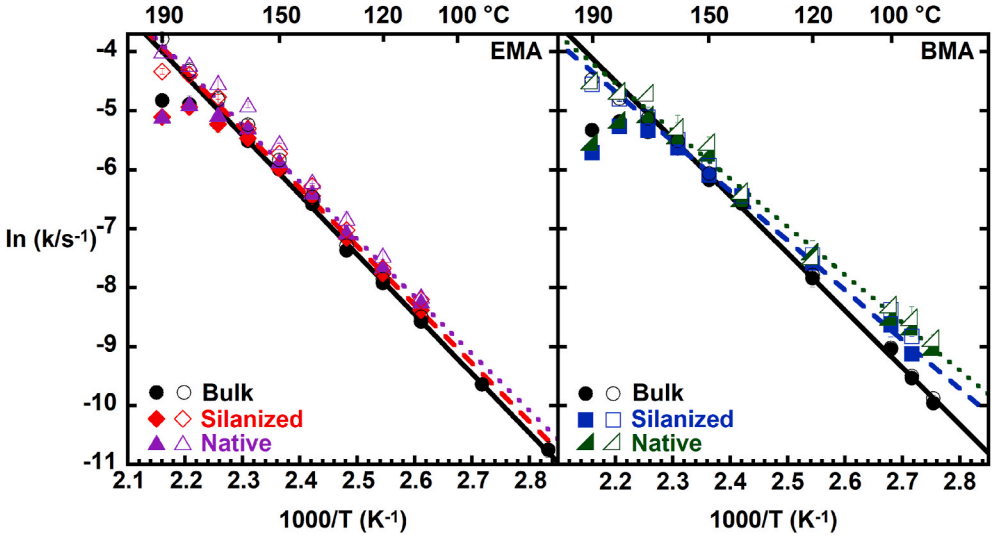

Fig. 3. Arrhenius plot for the effective rate constant prior to autoacceleration for bulk and nanoconfined samples of EMA (left) and BMA (right). Filled symbols represent data from Equation (3) ignoring the back reaction, and open symbols represent data from Equation (5) considering the back reaction, with circles representing the bulk samples, diamonds and squares indicating samples in 8 nm silanized pores, and triangle and right triangle indicating samples in 8 nm native pores. The lines are Arrhenius fits up to 150 °C with the solid line representing the bulk, the dashed line representing samples in silanized nanopores, and the dotted line representing samples in native nanopores. View in color for best clarity. (For interpretation of the references to color in this figure legend, the reader is referred to the Web version of this article.)

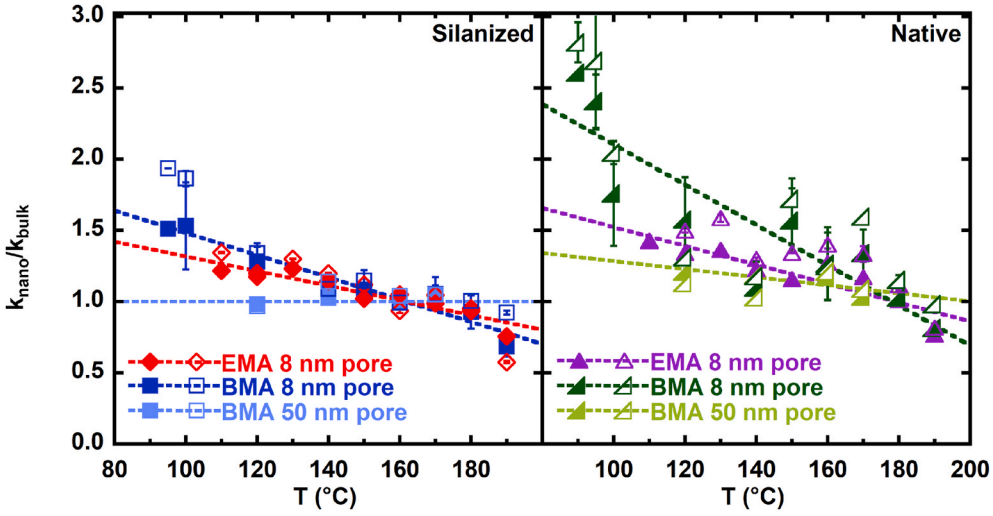

Fig. 4. The effective rate constant prior to autoacceleration normalized by the bulk value for nanoconfined samples as a function of polymerization temperature for reactions confined to silanized (left) and native (right) pores. Calculations based on Equation (3) are shown as filled symbols and those from equation (5) are shown as open symbols. Red diamonds and purple triangles are results for EMA samples in 8 nm pores. Blue squares and green right triangles are results for BMA samples in 8 nm pores. Light blue squares and light green right triangles are results for BMA samples in 50 nm pores. The lines are only guides to the eye. View in color for best clarity. (For interpretation of the references to color in this figure legend, the reader is referred to the Web version of this article.)

simulations, and the results have been ascribed to increased T_g in the nanopores, as well as to the presence of an immobile or slower layer at the nanopore or substrate surface [47–51], with larger reductions for stronger interactions between the fluid and the surface [51]; we similarly observed an increase in the glass transition of PMMA in 13-nm pores, with native pores showing a larger effect with T_g 15 °C higher than bulk [8]. We note that the effective viscosity of polymers may also decrease in nanopores [48,50–52] due to plug flow when reptation motion rather than flow dominates under nanoconfinement [48], due to slip at the pore surface [51], or, in the case of polymeric thin films, due to mobility at the free surface [50]; however, these mechanisms are not expected to dominate in our system since we do not have pressure-driven flow or a free surface.

The time to reach autoacceleration, t_{gel}, decreases dramatically with increasing temperature, as shown in Fig. 5b. The temperature dependence of t_{gel} depends on both the temperature dependence of x_{gel} and the effective reaction rate constant k_{eff} with the effect of temperature dominating due to the Arrhenius temperature dependence. In fact, the data in Fig. 5 can be described by Arrhenius functions using apparent activation energies that are approximately 9–30% lower than those that describe k_{eff}. The onset of autoacceleration clearly occurs earlier under nanoconfinement for both EMA and BMA systems, with polymerizations in native pores showing the most pronounced effects. Interestingly, the values of x_{gel} and t_{gel} are approximately the same for EMA and BMA, indicating that, similar to the bulk case, the length of the alkyl group does not affect the onset of autoacceleration. Again, this effect is ascribed to i) the two systems having similar T_gs at the onset of autoacceleration (due to the low conversion x_{gel} and the similar T_gs of the monomers) and ii) the reaction temperature being very far above the glass transition such that small changes in T-T_g do not have a significant impact on mobility.

The natural logarithm of the induction time is plotted as a function of reciprocal temperature in Fig. 6. As temperature decreases, the induction time, increases. Only data at and below 120 °C is presented since the induction time becomes insignificant at temperatures higher than 120 °C. Nanoconfinement increases the induction time and the effect is stronger in native pores, similar to the trend observed previously for MMA polymerization in 13 nm pores [16], although the increase appears to be more obvious in the current study perhaps due to different initiator and/or smaller pore size. The induction time follows an Arrhenius-type temperature behavior with an activation energy of 115 ± 9 kJ/mol, lower than the 144 ± 1 kJ/mol found in our previous work on MMA polymerization [16], but in both cases, higher than the overall activation energy value for the reaction.

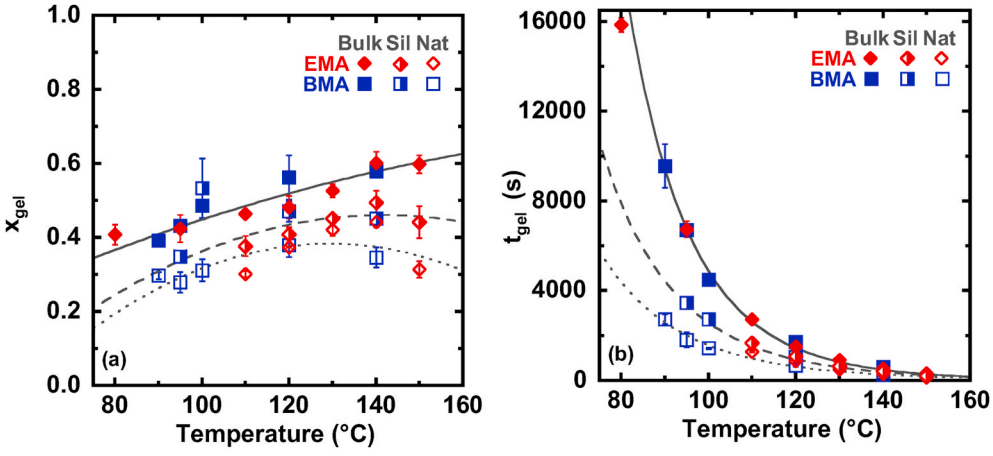

Fig. 5. (a) Conversion (x_{gel}) at the onset of autoacceleration and (b) time (t_{gel}) at the onset of autoacceleration as a function of polymerization temperature for EMA (red diamonds) and BMA (blue squares). Filled symbols indicate bulk samples, half-filled symbols indicate samples in silanized (sil) nanopores, and open symbols indicate samples in native (nat) nanopores. The lines are only guides to the eye with the solid line representing the bulk sample, the dashed line representing the samples in silanized nanopores, and the dotted line representing the samples in native nanopores. View in color for best clarity. (For interpretation of the references to color in this figure legend, the reader is referred to the Web version of this article.)

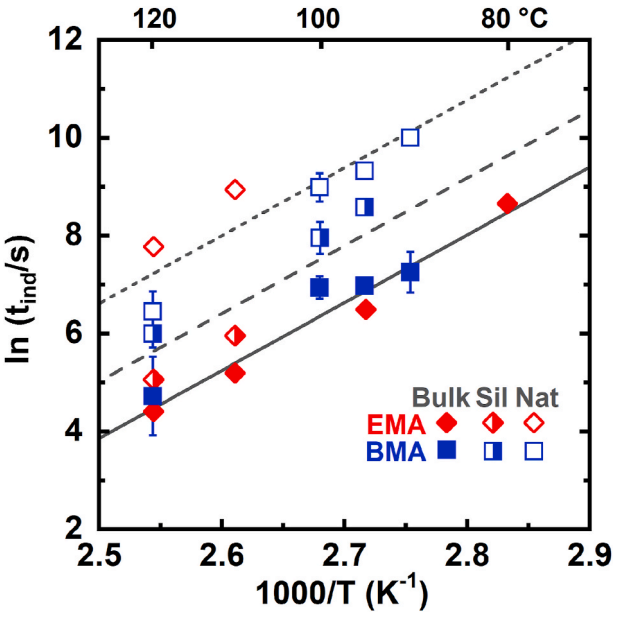

Fig. 6. The induction time for bulk and nanoconfined samples as a function of reciprocal temperature for EMA (red diamonds) and BMA (blue squares). Filled symbols indicate bulk samples, half-filled symbols indicate samples in silanized (sil) nanopores, and open symbols indicate samples in native (nat) nanopores. The lines are only guides to the eye with the solid line representing the bulk sample, the dashed line representing the samples in silanized nanopores, and the dotted line representing the samples in native nanopores. View in color for best clarity. (For interpretation of the references to color in this figure legend, the reader is referred to the Web version of this article.)

4. Discussion

The effective rate constants for the nanoconfined EMA and BMA polymerizations in 8 nm silanized pores are larger than those for bulk conditions, in contrast with our previous work of MMA polymerization in 13 nm silanized pores, where the effective rate constant for silanized samples was unchanged compared with bulk samples within experimental error [16]. The current system differs from the previous MMA polymerization in the temperature range, monomer, initiator, and pore size. A comparison of the apparent activation energy as a function of reciprocal diameter is plotted in Fig. 7 for EMA and BMA using the left-hand axis; our previous MMA results are also plotted in Fig. 7 using the right-hand axis which is shifted downwards by 12 kJ/mol [36] in order to account for the difference between the activation energy for decomposition E_d for the initiator AIBN used for MMA [16] and DtBP used in current study. In silanized pores, the apparent activation energy appears to be a stronger function of pore diameter for BMA than for EMA or MMA, with the trend possibly being a function of alkyl chain length in these three n-alkyl methacrylates. On the other hand, in native pores, the apparent activation energy appears to be a weaker function of pore diameter for EMA and BMA than for MMA, indicating that the interaction between the monomer and pore surface becomes weaker as the alkyl group length increases. One possible reason for this latter result could be due to the temperature ranges investigated for these systems as our previous work on MMA was limited to below 100 °C. As temperature increases, for example, specific interactions between the methacrylate group and silanol groups on the pore surface may weaken, similar to the decreasing strength of hydrogen bonding in water as temperature increases [53].

As shown in Fig. 3, the effective rate constants based on Equations (3) and (5) differ at temperatures higher than 160 °C, with the former significantly deviating from Arrhenius expectations indicating that the effect of depropagation becomes more appreciable. From Equation (4), the ratio of the rates of depropagation to propagation, R_{dp}/R_p, can be derived as:

$$\frac{R_{dp}}{R_p} = 1 - \frac{k_{eff}}{k_{Arr}} \tag{8}$$

where k_{eff} is the rate constant from Equation (3), assuming no back reaction, and k_{Arr} is the rate constant expected from the Arrhenius plot in the absence of the back reaction (which could also be given by the rate constant from Equation (5), although here we use the extrapolated Arrhenius value). The resulting ratio of the rates of depropagation and propagation is plotted as a function of polymerization temperature in Fig. 8. For both EMA and BMA, the depropagation rate is not significant until 160 °C, above which the ratio of the depropagation rate and propagation rate $\frac{R_{dp}}{R_p}$ increases as the polymerization temperature increases, consistent with the previous results in Fig. 3. The ratio of depropagation to propagation is larger than in the bulk at temperatures above 160 °C for EMA, whereas for BMA, this is the case only at the highest temperature studied. In addition, the relative rate versus temperature can be fitted using an Arrhenius expression, where the apparent activation energy is related to the difference in the activation energies of depropagation and propagation. For both nanoconfined cases, the difference in activation energies is larger than that in the bulk, with an

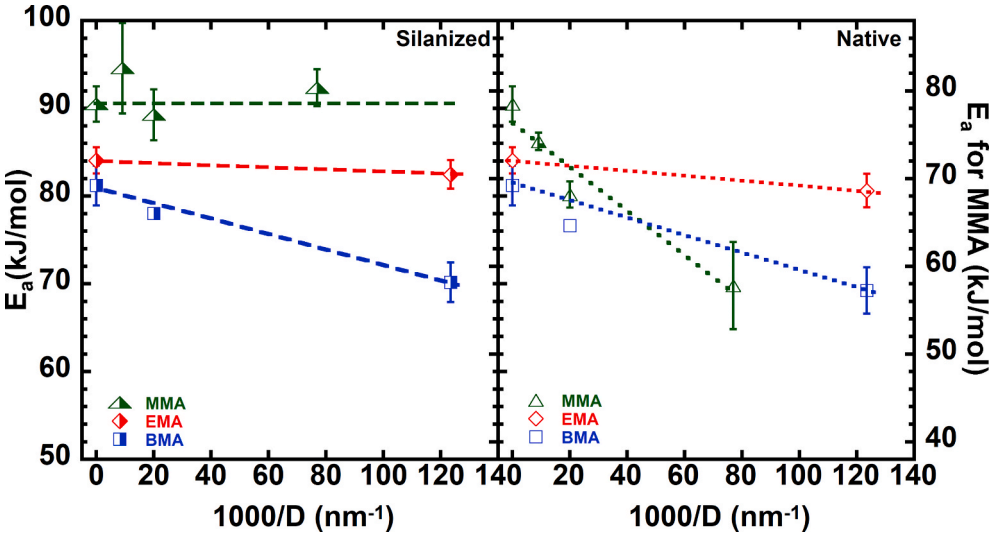

Fig. 7. Apparent activation energy for reaction as a function of reciprocal pore size for EMA (red symbols) and BMA (blue symbols) using the left-hand axis, with our previous MMA results (green symbols) [16] plotted using the right-hand axis which is shifted downwards by 12 kJ/mol to account for the different initiators used. Half-filled symbols indicate samples in silanized nanopores (on left), and open symbols indicate samples in native nanopores (on right). The error bars are the standard errors of the fitted parameter from the Arrhenius fit. Lines are only guides to the eye. View in color for best clarity. (For interpretation of the references to color in this figure legend, the reader is referred to the Web version of this article.)

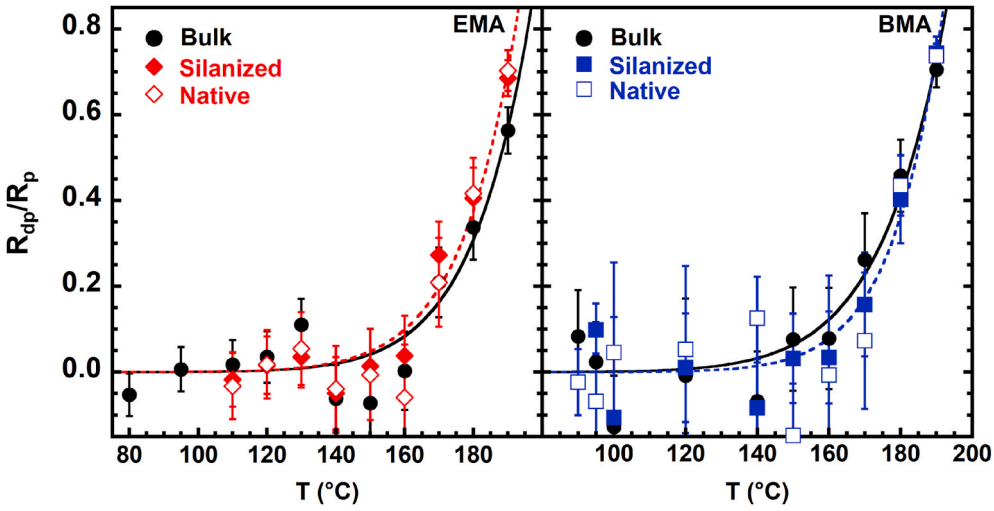

Fig. 8. The ratio of depropagation rate and propagation rate as a function of polymerization temperature for EMA and BMA. Black dots represent the bulk samples, full diamonds and squares indicate the samples confined in 8 nm silanized pores and open diamonds and squares indicate the samples confined in 8 nm native pores. The solid and dotted lines are presented only as guides to the eye for bulk and nanoconfined samples, separately.

increase of 26% for BMA, indicating that under nanoconfinement, depropagation will become even more significant relative to propagation as temperature increases.

5. Conclusions

The free radical polymerizations of ethyl- and n-butyl-methacrylate have been investigated in bulk and nanoconfinement conditions over a broad temperature range from 80 to 190 °C using di-*tert*-butyl peroxide (DtBP) as a thermal initiator. For bulk EMA and BMA, the initial reaction rates and autoacceleration becomes more significant with decreasing temperature. The effective rates are similar for the two monomers, but the BMA reacts approximately 11% faster at 95 °C. The times and conversions to reach autoacceleration are also similar for bulk EMA and BMA polymerizations, although the increase in the reaction rate at autoacceleration is much higher for EMA. In both cases, the conversion to reach autoacceleration x_{gel} increases slightly with increasing temperature, whereas the time to reach autoacceleration t_{gel} decreases dramatically. As temperature increases towards the ceiling temperature, the depropagation effect becomes more significant, consistent with prior results from other researchers.

Regarding the effect of nanopore confinement on EMA and BMA polymerization, the effective rates constants are highest in native pores and lowest in bulk conditions for both EMA and BMA, with the rates in silanized pores lying in the middle. The ratio of the effective rate constants of the nanoconfined and bulk samples, k_{nano}/k_{bulk}, decreases with increasing temperature and shows a stronger nanoconfinement effect in BMA than EMA. The onset of autoacceleration occurs earlier under nanoconfinement for both EMA and BMA systems, resulting in x_{gel} and t_{gel} showing the largest values in bulk samples and smallest values in native samples. The induction time follows Arrhenius behavior and increases under nanoconfinement. The apparent activation energy under nanoconfinement decreases as compared to the bulk for BMA. When compared to MMA, the apparent activation energy in silanized pores appears to be a stronger function of pore diameter for EMA and BMA than for MMA, with the trend appearing to be a function of alkyl chain length in these three n-alkyl methacrylates. On the other hand, in native pores, the apparent activation energy is a weaker function of pore diameter for EMA and BMA than for MMA presumably due to the higher temperature range investigated in present work. At high temperatures, as the ceiling temperature is approached, the ratio of the depropagation rate and propagation rate, $\frac{R_{dp}}{R_p}$, increases with the effect being more pronounced for the nanoconfined reactions.

CRediT authorship contribution statement

Qian Tian: Formal analysis, Data curation, Writing - original draft, Writing - review & editing. **Haoyu Zhao:** Formal analysis, Data curation, Writing - original draft, Writing - review & editing. **Sindee L. Simon:** Supervision, Writing - original draft, Writing - review & editing, Funding acquisition.

Declaration of competing interest

The authors declare that they have no known competing financial interests or personal relationships that could have appeared to influence the work reported in this paper.

Acknowledgment

Funding from the National Science Foundation DMR-1610614 and DMR-2004960 is gratefully acknowledged. The authors thank Dr. Yung P. Koh for instrumental support.

References

[1] J.L. Keddie, R.A.L. Jones, R.A. Cory, Interface and surface effects on the glass-transition temperature in thin polymer films, Faraday Discuss 98 (1994) 219–230.
[2] J.A. Forrest, K. Dalnoki-Veress, J.R. Stevens, J.R. Dutcher, Effect of free surfaces on the glass transition temperature of thin polymer films, Phys. Rev. Lett. 77 (1996) 2002–2005.
[3] M. Alcoutlabi, G.B. McKenna, Effects of confinement on material behaviour at the nanometre size scale, J. Phys. Condens. Matter 17 (2005) R461–R524.
[4] X.C. Li, T.A. King, F. Pallikari-Viras, Characteristics of composites based on PMMA modified gel silica glasses, J. Non-Cryst. Solids 170 (1994) 243–249.
[5] S.M. Ng, S. Ogino, T. Aida, K.A. Koyano, T. Tatsumi, Free radical polymerization within mesoporous zeolite channels, Macromol. Rapid Commun. 18 (1997) 991–996.
[6] T. Uemura, Y. Ono, K. Kitagawa, S. Kitagawa, Radical polymerization of vinyl monomers in porous coordination polymers: nanochannel size effects on reactivity, molecular weight, and stereostructure, Macromolecules 41 (2008) 87–94.
[7] K. Kageyama, J.-I. Tamazawa, T. Aida, Extrusion polymerization: catalyzed synthesis of crystalline linear polyethylene nanofibers within a mesoporous silica, Science 285 (1999) 2113–2115.
[8] H.Y. Zhao, Z.N. Yu, F. Begum, R.C. Hedden, S.L. Simon, The effect of nanoconfinement on methyl methacrylate polymerization: T_g, molecular weight, and tacticity, Polymer 55 (2014) 4959–4965.
[9] S. Amanuel, V.M. Malhotra, Effects of physical confinement (< 125 nm) on the curing behavior of phenolic resin, J. Appl. Polym. Sci. 99 (2006) 3183–3186.
[10] Q.X. Li, S.L. Simon, Curing of bisphenol M dicyanate ester under nanoscale constraint, Macromolecules 41 (2008) 1310–1317.

[11] Q.X. Li, S.L. Simon, Surface chemistry effects on the reactivity and properties of nanoconfined bisphenol M dicyanate ester in controlled pore glass, Macromolecules 42 (2009) 3573–3579.
[12] E. Lopez, S.L. Simon, Trimerization reaction kinetics and T_g depression of polycyanurate under nanoconfinement, Macromolecules 48 (2015) 4692–4701.
[13] B. Sanz, N. Ballard, Á. Marcos-Fernández, J.M. Asua, C. Mijangos, Confinement effects in the step-growth polymerization within AAO templates and modeling, Polymer 140 (2018) 131–139.
[14] M. Tarnacka, M. Dulski, S. Starzonek, K. Adrjanowicz, E.U. Mapesa, K. Kaminski, M. Paluch, Following kinetics and dynamics of DGEBA-aniline polymerization in nanoporous native alumina oxide membranes–FTIR and dielectric studies, Polymer 68 (2015) 253–261.
[15] B. Yancey, S. Vyazovkin, Venturing into kinetics and mechanism of nanoconfined solid-state reactions: trimerization of sodium dicyanamide in nanopores, Phys. Chem. Chem. Phys. 16 (2014) 11409–11416.
[16] H.Y. Zhao, S.L. Simon, Methyl methacrylate polymerization in nanoporous confinement, Polymer 52 (2011) 4093–4098.
[17] M. Tarnacka, A. Dzienia, P. Maksym, A. Talik, A. Zieba, R. Bielas, K. Kaminski, M. Paluch, Highly efficient ROP polymerization of ε-caprolactone catalyzed by nanoporous alumina membranes. How the confinement affects the progress and product of ROP reaction, Macromolecules 51 (2018) 4588–4597.
[18] M. Tarnacka, P. Maksym, A. Zięba, A. Mielańczyk, M. Geppert-Rybczyńska, L. Leon-Boigues, C. Mijangos, K. Kamiński, M. Paluch, The application of spatially restricted geometries as a unique route to produce well-defined poly (vinyl pyrrolidones) via free radical polymerisation, Chem. Commun. 55 (2019) 6441–6444.
[19] B. Sanz, N. Ballard, J.M. Asua, C. Mijangos, Effect of confinement on the synthesis of PMMA in AAO templates and modeling of free radical polymerization, Macromolecules 50 (2017) 811–821.
[20] S. Qavi, A. Bandegi, M. Firestone, R. Foudazi, Polymerization in soft nanoconfinement of lamellar and reverse hexagonal mesophases, Soft Matter 15 (2019) 8238–8250.
[21] X. Xu, Y.N. Zeng, C.L. Yu, F.A. Zhang, Controlled RAFT polymerization of MMA in confined space of various pore sizes of SBA-15, J. Porous Mater. 27 (2020) 95–105.
[22] T. Cui, J.D. Ding, J.Z.Y. Chen, Dynamics of a self-avoiding polymer chain in slit, tube, and cube confinements, Phys. Rev. E - Stat. Nonlinear Soft Matter Phys. 78 (2008), 061802.
[23] F. Begum, S.L. Simon, Modeling methyl methacrylate free radical polymerization in nanoporous confinement, Polymer 52 (2011) 1539–1545.
[24] H.N. Wang, Y.W. Qiang, A.A. Shamsabadi, P. Mazumder, K.T. Turner, D. Lee, Z. Fakhraai, Thermal degradation of polystyrene under extreme nanoconfinement, ACS Macro Lett. 8 (2019) 1413–1418.
[25] K.F. O'Driscoll, A.F. Burczyk, Kinetics of styrene and methylmethacrylate polymerizations in a starved feed reactor, Polym. React. Eng. 1 (1993) 111–144.
[26] R.A. Hutchinson, D.A. Paquet, S. Beuermann, J.H. McMinn, Investigation of methacrylate free-radical depropagation kinetics by pulsed-laser polymerization, Ind. Eng. Chem. Res. 37 (1998) 3567–3574.
[27] D. Kukulj, T.P. Davis, Average propagation rate coefficients in the free-radical copolymerization of styrene and α-methylstyrene measured by pulsed-laser polymerization, Macromolecules 31 (1998) 5668–5680.
[28] H.Y. Zhao, S.L. Simon, Equilibrium free-radical polymerization of methyl methacrylate under nanoconfinement, Polymer 66 (2015) 173–178.
[29] C.L. Jackson, G.B. McKenna, The melting behavior of organic materials confined in porous solids, J. Chem. Phys. 93 (1990) 9002–9011.
[30] V. Erb, Diploma thesis, Max-Planck-Institut fur Polymerforschung, Mainz (1993).
[31] S.L. Simon, J.W. Sobieski, D.J. Plazek, Volume and enthalpy recovery of polystyrene, Polymer 42 (2001) 2555–2567.
[32] R.E. Cook, K.J. Ivin, The equilibrium between ethyl methacrylate and its polymer, Trans. Faraday Soc. 53 (1957) 1132–1135.
[33] F.S. Dainton, K.J. Ivin, D.A.G. Walmsley, The heats of polymerization of some cyclic and ethylenic compounds, Trans. Faraday Soc. 56 (1960) 1784–1792.
[34] L.K.J. Tong, W.O. Kenyon, Heats of polymerization. II. Some esters of α-methylacrylic acid, J. Am. Chem. Soc. 68 (1946) 1355–1357.
[35] K.G. McCurdy, K.J. Laidler, Thermochemical studies of some acrylate and methacrylate polymerizations in emulsion systems, Can. J. Chem. 42 (1964) 818–824.
[36] G. Odian, Principles of polymerization; 4th, in: John Wiley & Sons (Ed.), 2004. New York.
[37] T. Otsu, T. Ito, M. Imoto, Vinyl polymerization. LXXIX. Effect of the alkyl group on the radical polymerization of alkyl methacrylates, J. Polym. Sci. - Part A Gen. Pap. 2 (1964) 2901–2906.
[38] N.A. Plate, A.G. Ponomarenko, Kinetic features of the radical polymerization of n-alkylmethacrylates, Polym. Sci. USSR 16 (1974) 3067–3081.
[39] S.L. Tomić, J.M. Filipović, J.S. Veličković, L. Katsikas, I.G. Popović, The polymerisation kinetics of lower dialkyl itaconates, Macromol. Chem. Phys. 200 (1999) 2421–2427.
[40] E.S. Huyser, R.M. VanScoy, Effects of solvent on the unimolecular decomposition of t-butyl peroxide, J. Org. Chem. 33 (1968) 3524–3527.
[41] C. Walling, D. Bristol, On the reality of solvent effects in the decomposition of tert-butyl peroxide, J. Org. Chem. 36 (1971) 733–735.
[42] S. Lora, G. Palma, L. Busulini, B. Castilletti, Application of a calorimetric method in radiation-induced polymerization—III: determination of propagation and termination rate constants for n-butyl methacrylate, Eur. Polym. J. 10 (1974) 1223–1227.
[43] J. Brandrup, E.H. Immergut, E.A. Grulke, A. Abe, D.R. Bloch, Polymer Handbook, fourth ed., Wiley, New York, 1989.
[44] S. Kim, J. Chen, T. Cheng, A. Gindulyte, J. He, S. He, Q. Li, B.A. Shoemaker, P. A. Thiessen, B. Yu, L. Zaslavsky, J. Zhang, E.E. Bolton, Nucleic Acids Res. 47 (D1) (2019) D1102–D1109, from, https://pubchem.ncbi.nlm.nih.gov/.
[45] M.K. Karabaev, T.P. Abduzhaminov, M.M. Kenisarin, A.A. Saidov, Thermodynamics of the crystal-liquid phase transition in acrylates and methacrylates. *Izv. Akad. Nauk uzb. SSR ser*, Fiz-Mat. Nauk 5 (1985) 74–77, from, https://webbook.nist.gov/.
[46] S. Rogers, L. Mandelkern, Glass transitions of the poly-(n-alkyl methacrylates), J. Phys. Chem. 61 (1957) 985–991.
[47] J.L. Hor, H.N. Wang, Z. Fakhraai, D. Lee, Effect of physical nanoconfinement on the viscosity of unentangled polymers during capillary rise infiltration, Macromolecules 51 (2018) 5069–5078.
[48] Y. Yao, H.-J. Butt, G. Floudas, J.J. Zhou, M. Doi, Theory on capillary filling of polymer melts in nanopores, Macromol. Rapid Commun. 39 (2018) 1800087.
[49] C.H. Tu, M. Steinhart, H.J. Butt, G. Floudas, In situ monitoring of the imbibition of poly(n-butyl methacrylates) in nanoporous alumina by dielectric spectroscopy, Macromolecules 52 (2019) 8167–8176.
[50] A. Shavit, R.A. Riggleman, The dynamics of unentangled polymers during capillary rise infiltration into a nanoparticle packing, Soft Matter 11 (2015) 8285–8295.
[51] D. Feng, X.F. Li, X.Z Wang, J. Li, T. Zhang, Z. Sun, M.X. He, Q. Liu, J.Z. Qin, S. Han, Capillary filling of confined water in nanopores: coupling the increased viscosity and slippage, Chem. Eng. Sci. 186 (2018) 228–239.
[52] L.G. Cencha, R. Urteaga, C.L.A. Berli, Interferometric technique to determine the dynamics of polymeric fluids under strong confinement, Macromolecules 51 (2018) 8721–8728.
[53] W.L. Jorgensen, J.D. Madura, Temperature and size dependence for Monte Carlo simulations of TIP4P water, Mol. Phys. 56 (1985) 1381–1392.